Networked ZnO nanosheets produced by automatic SILAR method *Author Accepted Manuscript*

Sergey Petrushenko
Faculty of Physics
V.N. Karazin Kharkiv National University; Technical University of Liberec
Kharkiv, Ukraine; Liberec, Czech Republic
petrushenkokhnu@gmail.com

Sergey Dukarov
Faculty of Physics
V.N. Karazin Kharkiv National University
Kharkiv, Ukraine
dsv@univer.kharkov.ua

Volodymyr Sukhov
Faculty of Physics
V.N. Karazin Kharkiv National University
Kharkiv, Ukraine
vsukhov@karazin.ua

Mateusz Fijalkowski
Institute for Nanomaterials, Advanced Technologies and Innovation
Technical University of Liberec
Liberec, Czech Republic
mateusz.fijalkowski@tul.cz

Natalia Klochko
Micro- and nanoelectronics department
National Technical University "Kharkiv Polytechnic Institute"
Kharkiv, Ukraine
klochko.np16@gmail.com

Volodymyr Kopach
Micro- and nanoelectronics department
National Technical University "Kharkiv Polytechnic Institute"
Kharkiv, Ukraine
Kopach@ kpi.kharkov.ua

***Abstract*— In this work, we have developed an automatic low temperature, cheap, simple and scalable chemical method Successive Ionic Layer Adsorption and Reaction (SILAR) to obtain layers of two-dimensional zinc oxide (ZnO) nanostructures from aqueous solutions. The ZnO networked nanosheets obtained by the automatic SILAR method have high adhesion to the glass substrate and improved mechanical resistance, which was confirmed by scratch adhesion tests performed by applying a progressive load. The value of the normal force Fz = 2.6 N, corresponding to the critical load Lc, for networked ZnO nanosheets is greater than for a conventional array of ZnO nanorods, for which Fz = 2.1 N.**

Keywords*— Zinc oxide, SILAR, networked nanosheet, 2D nanostructure, scratch testing, SEM

I. INTRODUCTION

Zinc oxide (ZnO) has a number of unique chemical and physical properties, including high chemical stability and photosensitivity [1], outstanding triboelectric and piezoelectric properties [2–4]. This makes it a key technological material among all metal oxides and causes its wide application in various fields [1–9]. Moreover, recently, many studies and experimental analyzes have improved the performance of ZnO materials for plenty of applications by creating zinc oxide nanostructures, especially two-dimensional (2D) forms such as nanoplates or nanosheets and nanopellets [2-8]. According to [4], two-dimensional ZnO nanosheets or nanoplates should be ideal components for nanoscale sensor applications, data storage in memory devices, and optoelectronics due to their nanometer thickness, high surface to volume ratio, and enhanced optical and photocatalytic activity. It is stated in [3, 4] that two-dimensional semiconductor nanostructures, such as nanosheets, nanoplates and nanowalls, also have good mechanical strength for use in triboelectric and piezoelectric energy conversion and storage devices, chemical and biological sensors, etc. As noted in [8], ZnO nanosheets are becoming an alternative to ZnO nanorods, since nanosheets are more flexible than nanorods. For example, the authors of [2] found a high charge density caused by the polarization of ZnO nanosheets under the action of a compressive force due to the piezoelectric effect. In [3] the coupled semiconducting and piezoelectric properties of the networked ZnO nanosheets turned out to be structurally stable under huge external mechanical loads in the efficient piezoelectric power generator for miniaturization of the power unit and autonomous power supply of nanorobots and devices implanted in the body.

Most technologies for growing ZnO are characterized by the predominant growth of the (0002) plane of zinc oxide. According to [6], owing to the special crystal structure of ZnO, rapid crystal growth along the <0001> direction is energetically favorable for ZnO due to the higher surface energy of the {0001} polar planes. Consequently, the intrinsic habit of ZnO nanocrystals looks like a hexagonal prism, and their arrays most often consist of nanorods, which are located perpendicular to the substrate or at different angles to it. However, in aqueous solutions, the conditions for the formation of a unique two-dimensional structure of ZnO nanosheets with the predominant growth of non-polar $(10\bar{1}0)$ ZnO crystal planes are realized by electrochemical deposition [2,6], and also by hydrothermal [7,8] and similar chemical solution methods such as Chemical Bath Deposition (CBD) [3,5,9]. For example, in the process of zinc oxide electrochemical deposition in [2], the slowdown of ZnO growth along the (0002) orientation, leading to the honeycomb network structure of ZnO nanosheets is explained by the presence of hexamethylenetetramine (HMTA) in the aqueous electrolyte as an additional source of OH^- ions. In [6], the growth of the $(10\bar{1}0)$ ZnO plane during electrodeposition is due to the presence of HMTA and the blocking of the (0002) ZnO plane by the adsorption of chloride ions from the aqueous electrolyte. The authors of [3,9] succeeded in growing the two-dimensional structure of ZnO nanosheets by wet chemical methods in aqueous solutions containing HMTA. In [4,5], wet chemical growth was used in a highly alkaline aqueous medium, in which superfluous OH^- ions are easily adsorbed on the positively charged (0001) surface of ZnO, and thus growth along the [0001] direction was limited to a certain extent to obtain networked ZnO nanosheets. The use of a ZnO seed layer at the initial stage additionally contributed to the creation of ZnO nanosheets, the axes of which were parallel to the substrate; thus, the ZnO plates were located almost vertically to the substrate [4,8].

MSCA4Ukraine project funded by the European Union and Ministry of Education and Science of Ukraine.

Wet chemical low-temperature, cheap, simple and scalable method Successive Ionic Layer Adsorption and Reaction (SILAR) is an evolution and combination of two deposition methods, namely Atomic Layer Deposition (ALD) and CBD [10]. The SILAR deposition uses a physically separated layer-by-layer approach similar to ALD, but carried out as CBD through precipitation from aqueous solutions in the environment at ambient pressure, without the need for high vacuum equipment. Unlike CBD, it uses alternating chemical precursor baths as well as additional pure water baths between precipitation cycles to remove excess precursor molecules [10]. The main advantage of SILAR over CBD is the ability to control the thickness of deposited layers by choosing the number of SILAR cycles. However, neither we [11, 12] nor other authors [10, 13, 14] have been able to obtain two-dimensional structures in the form of networked ZnO nanosheets using the manual SILAR approach, which has been used so far to deposit zinc oxide films [10-14]. In this work, we demonstrate for the first time layers of networked ZnO nanosheets fabricated by the automatic SILAR method using a ZnO seed layer at the initial stage of nucleation. The high adhesion of ZnO nanosheets to the glass substrate and their improved mechanical resistance are confirmed by scratch adhesion tests performed by applying a progressive load.

II. EXPERIMENTAL PROCEDURES

All chemicals in this work were of analytical grade. Glass plates with an active area of 2.5 cm × 5 cm were used as substrates. They were cleaned by soaking overnight in a 10% aqueous solution of Elma lab clean A20sf (ELC A20sf) surfactant-free cleaning concentrate suitable for aqueous cleaning of laboratory glassware. Then the substrates were successively washed in a flow of distilled water, in acetone, and in ethanol. To apply ZnO layers only on one side of the substrate, two glass plates were tightly pressed against each other and fixed in the holder, so that the solutions did not penetrate to the inner side of the glass substrate. Thanks to this, it was possible to obtain two samples under the most identical conditions within one experimental cycle. Typically, one ZnO layer was deposited by the SILAR method on a bare glass substrate, and the second one was deposited on a glass substrate coated with a ZnO seed layer. Thus, the effect of the seed layer on the morphology and properties of the nanostructured zinc oxide layer obtained by the SILAR method was most convincingly tested.

To prepare the seed layer of ZnO, we used an aqueous solution with a tetraamine zinc complex $[Zn(NH_3)_4]^{2+}$ obtained by dissolving 0.05 M ZnO in an ammonia solution (NH_4OH) until pH 10.3 was reached. Then the substrates were immersed in the seed solution for 30 s, and dried in a hot air stream. This process was repeated 10 times to obtain ZnO seed layer that uniformly covered the glass surface.

In this study, to deposit ZnO films via SILAR method we used cationic precursor contained aqueous solution of zinc sulfate (1 M $ZnSO_4$) dissolved in NH_4OH. To prepare it, 25% NH_4(OH solution was added slowly to the aqueous $ZnSO_4$ solution This initially formed $Zn(OH)_2$ precipitate, but in excess ammonia (at pH 12.1), it turned into a colorless transparent solution containing tetraamine zinc complex $[Zn(NH_3)_4]^{2+}$. Hot (85–90°C) distilled water was used as an anionic precursor. To obtain good reproducibility of ZnO films, we developed an automatic SILAR method based on the use of an universal motorized platform with computer numerical control (CNC), which photograph is presented in Fig. 1. Similar platforms are widely used in conventional commercial 3D printers. Using a g-code, all steps of the SILAR method were programmed, and reproducibility of the substrate immersion speed and time of each deposition step was ensured with an error of < 0.1 %. One growth SILAR cycle included the following three stages. The first stage consisted in immersing the glass substrate in a solution of the $[Zn(NH_3)_4]^{2+}$ cationic precursor for 10 s. The second step consisted of immersing in hot distilled water for 10 seconds, while stirring with a magnetic stirrer at 100 rpm after five SILAR cycles (samples No 1 and No 2) or all the time (samples No 3 and No 4). The third stage was a rinsing in distilled water at room temperature for 5 seconds to remove excess ions and weakly bound particles from the substrate.

In 50 SILAR cycles, we have grown nanostructured ZnO layers. Samples No 1 and No 3 were prepared without seed layers, while samples No 2 and No 4 were prepared with ZnO seed layers. The average thickness t in the range of ~4-16 μm was determined gravimetrically without taking into account the network morphology of the zinc oxide layers, but assuming their density equal to the bulk density of ZnO 5.61 g/cm^3. In addition, the thickness $t^{\#}$ of SILAR-produced ZnO films, including layers of 2D ZnO nanosheets, was estimated taking into account their network morphology using scanning electron microscopy (SEM) in the secondary electron mode. For this, by reducing the distance between the sample and the objective lens as much as possible, the minimum depth of focus of the microscope was ensured. Then, while observing the edge of the sample, the electron probe was sequentially focused on the surface of the sample and the substrate. The difference in focal lengths between these two observations was taken equal to the film thickness.

The morphology of the ZnO layers deposited by the automatic SILAR method was studied using SEM images obtained with a scanning electron microscope "TESCAN, Vega3 SBU" operating at an accelerating voltage of 30 kV.

UV-Vis-NIR transmittance spectra $T(\lambda)$ for ZnO layers were obtained on a LAMBDA 35 PerkinElmer spectrophotometer in the wavelength range λ 300-1100 nm. Pure glass plates were used as control samples. Optical band gaps E_g of ZnO layers were determined from their absorption coefficients (α) calculated as described in [15]:

Fig. 1. Photograph of the ZnO deposition process by the automatic SILAR method using an universal motorized platform with computer numerical control

$$a = (-\ln T)/t \quad (1)$$

The value of Eg was estimated using the classical relationship between the absorption coefficient and the photon energy (hv) according to the relation [13-15]:

$$(a \cdot hv)^2 = A_0 \cdot (hv - E_g) \quad (2)$$

where A_0 is a constant. Due to the nanostructured nature of the ZnO layers, it was difficult to unambiguously determine their thickness. Therefore, for the graphical determination of the band gap, we used the dependence $(-\ln T \cdot hv)^2$ from hv. E_g was obtained by extrapolating the linear portion of the dependence $(-\ln T \cdot hv)^2$ on hv.

To evaluate the adhesion and mechanical resistance of the nanostructured ZnO layers deposited via SILAR on glass substrates, we used a scratch adhesion testing performed by applying a progressive load, as described in [16-18]. The scratch tester "Bruker UMT-2MT-2" was used in the mode of linear force increase. It was equipped with a moveable table and transducers for recording two forces: vertical (normal) force (F_z) and horizontal (tangential) (F_x) force, – while the indenter was pressed onto the surface and simultaneously drawn over it. A progressively increased load was strictly controlled by the programmable electronic device. Thus, as the normal force increased, the table with the sample moved at a constant speed v 0.2 mm/s in the horizontal direction. Since the tangential force was equal to the friction force, the recorded friction coefficient ((μ) of the indenter was determined as the ratio of F_x required to displace the sample relative to the table, to the normal force F_z pressing the indenter ($\mu \approx F_x/F_z$) [18].

According to schematic in Fig. 2, we used a stylus having a Rockwell Diamond indenter with a radius of curvature of 200 μm. The value of the normal force F_z of 0.5 N was chosen as a criterion for the contact of the indenter with the ZnO surface. The F_z increased linearly in the range from 2 to 20 N for 25 s or 2 to 10 for 10 s, depending on the selected mode. The indentor track and the failure events were examined by an optical microscope. The indenter immersion depth Z, the friction coefficient μ, and the acoustic emission (AE) arising from the destruction of the ZnO and glass were also recorded during scratch testing. Each scratch test was repeated four times. Critical load (L_c) corresponded to the destruction of the ZnO layer According to [16,17], the L_c value determined the adhesion strength.

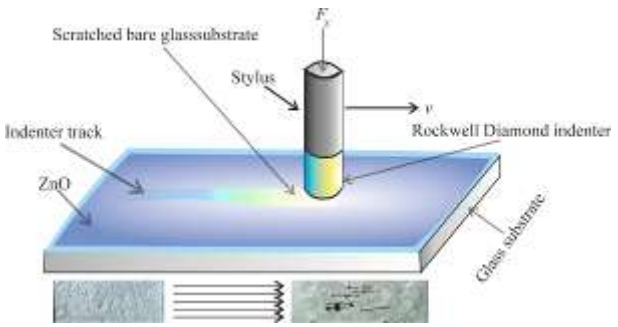

Fig. 2. The upper part of the figure shows a schematic of the setup for scratch adhesion tests, carried out with the application of a linearly increasing normal force F_z and with a diamond indenter displaced at a constant speed v relative to the ZnO layer deposited on the glass substrate

III. Results and Discussion

Fig. 3 and Fig. 4 present SEM images demonstrating the effect of ZnO seed layers and stirring of the anionic precursor (hot (85–90°C) water) during SILAR deposition. As seen in Fig. 3 (a,b) and Fig. 4 (a,b), without seed layers, disordered arrays of hexagonal nanorods were obtained, which are characteristic of ZnO films deposited by the SILAR method in different laboratories [10–15]. Comparison Fig. 3 and Fig. 4 shows that stirring of the anionic precursor during all fifty SILAR cycles contributed to better purification of the growing zinc oxide layer from excess ions and weakly bound particles. In addition, the stirring of the anionic precursor during the entire time made it possible to slightly decrease the average diameter of zinc oxide nanorods from 345 nm in Fig. 3 (a,b) to 306 nm in Fig.4 (a,b).

SEM images in Figs. 3 (c,d) and 4 (c,d) confirmed that the coating of glass substrates with ZnO seeds makes it possible to radically change the morphology of zinc oxide layers deposited by the automatic SILAR method, turning them into networked ZnO nanosheets. A possible cause may be the alkaline solution for preparing the ZnO seed layers. In accordance with described in [4,8], an excess of OH^- ions adsorbed on the positively charged (0001) ZnO surface limits the growth in the [0001] direction and promotes the preferential growth of nonpolar $(10\bar{1}0)$ ZnO crystal planes. Two-dimensional ZnO nanosheets obtained by the automatic SILAR method have average linear dimensions of ~22 μm if the anionic precursor was stirred only after five SILAR cycles, and ~8 μm if the anionic precursor was stirred during all SILAR cycles.

Accordingly, the thickness of a single ZnO nanosheet also decreased with stirring from ~390 μm in Fig. 3 (d) to ~47 μm in Fig. 4 (d). Thus, the automatic SILAR method developed here made it possible not only to obtain a promising material from networked ZnO nanosheets. In addition, this method offers the possibility of simple control of the geometric dimensions of 2D ZnO nanostructures by changing the modes of solution stirring. At the same time, as can be seen from Table. 1, due to the seed layers and continuous stirring of the anionic solution, the thickness t of the ZnO layers increased regularly.

The thicknesses $t^{\#}$ of the SILAR-deposited ZnO layers, estimated using scanning electron microscopy, were much larger, than t. For example, sample No 3 has $t^{\#}$ =100 μm and sample No 4 has $t^{\#}$ =70 μm. These data are related to the highly porous network structure of the ZnO layers. Due to the large thickness and nanoscale network structure associated with diffuse scattering and diffuse reflection of light, all presented in Fig. 5 (a) zinc oxide layers are translucent. The optical band gaps of ZnO films obtained using SILAR are in the range of 3.05 – 3.16 eV (Fig. 5 (b), Table 1), which is typical for direct allowed optical transitions in nanostructured ZnO layers without quantum confinement effect [13–15].

The scratch test with a linear increase in force makes it possible to determine, in accordance with proposed in [16-19], the failure modes inside ZnO layers deposited by the SILAR method, at their boundaries with glass substrates, and inside glass plates as a result of the action of tensile stresses during displacement and indentation diamond tip of the indentor.

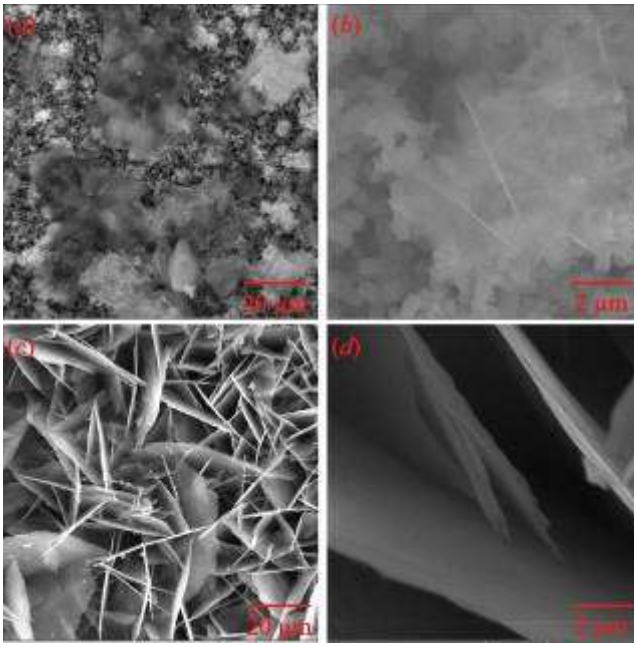

Fig. 3. SEM images of ZnO layers deposited by the SILAR method on bare glass substrates (sample No 1) (a, b) and on glass substrates coated with ZnIO seed layers (sample No 2) (c, d) with anionic precursor stirring switched on after five SILAR cycles

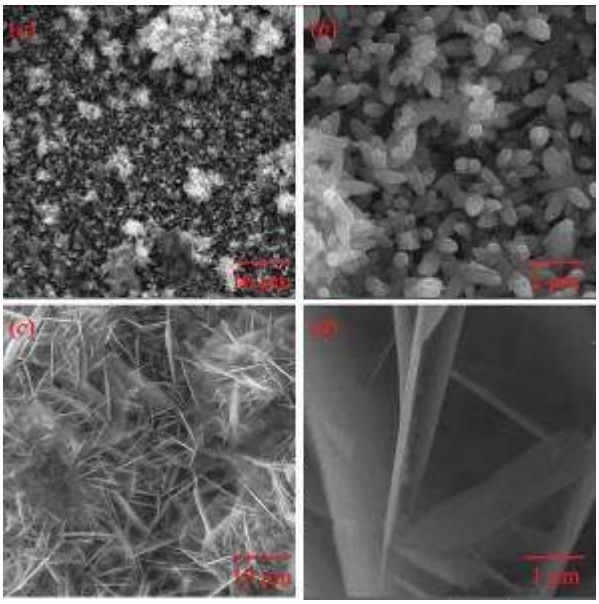

Fig. 4. SEM images of ZnO layers deposited by the SILAR method on bare glass substrate (sample No 3) (a, b) and on glass substrate coated with ZnO seed layer (sample No 4) (c, d) with stirring of the anionic precursor during all SILAR cycles

SEM images in Fig. 6 (a) and (c) show the results of scratching sample No 3, which consists of arrays of disordered hexagonal ZnO nanorods deposited on the bare glass substrate. SEM images in Fig. 6 (b) and (d) demonstrate the scratching of sample No 4 with networked ZnO nanosheets obtained by the SILAR method on the glass substrate coated with ZnO seed layer.

We can see in Fig. 6 (a) and (b) scratch tracks, the widths of which are 80 μm and 55 μm, respectively. These width data coincide with the data of optical microscopy in Fig. 8. The scratch tracks in Fig. 6 (a) and (b) extend deep into the glass substrate. According to [16], this failure mode is typical for the splitting of the brittle substrate due to good adhesion between the coating and the substrate, in our case, at the glass–ZnO interface. Thus, good adhesion between glass and zinc oxide is observed for both samples. The narrower scratch track for the sample No 4 with networked ZnO nanosheets confirms the increased strength of this material.

According to [16], both tensile and compressive stresses were induced in the coating-substrate system during the test and so a complex interplay between all the possible failure modes can be expected. Abrasion of zinc oxide nanostructures and their cracking in the contact area, revealed on SEM images after scratch adhesion tests in Figs. 6 are due to tensile stresses during sliding of the diamond indenter.

We can see in Fig. 6 (a) and (b) scratch tracks, the widths of which are 80 μm and 55 μm, respectively. These width data coincide with the data of optical microscopy in Fig. 8. The scratch tracks in Fig. 6 (a) and (b) extend deep into the glass substrate. According to [16], this failure mode is typical for the splitting of the brittle substrate due to good adhesion between the coating and the substrate, in our case, at the glass–ZnO interface. Thus, good adhesion between glass and zinc oxide is observed for both samples. The narrower scratch track for the sample No 4 with networked ZnO nanosheets confirms the increased strength of this material.

According to [16], both tensile and compressive stresses were induced in the coating-substrate system during the test and so a complex interplay between all the possible failure modes can be expected. Abrasion of zinc oxide nanostructures and their cracking in the contact area, revealed on SEM images after scratch adhesion tests in Figs. 6 are due to tensile stresses during sliding of the diamond indenter.

Tensile cracking of ZnO in the form of partial ring cracks occurs along the sides of the indenter and manifests itself as cracks at the track edge parallel and perpendicular to the scratch direction (Fig. 6 (a) and (b)).

TABLE I. THICKNESSES AND BAND GAPS OF THE NANOSTRUCTURED ZNO LAYERD DEPOSITED BY THE SILAR METHODS USING DIFFERENT MODES

ZnO sample	**ZnO deposition mode, thickness and band gap**		
	SILAR mode and ZnO morphology	***t, μm***	***E_g, eV***
No 1	ZnO nanorods on bare glass substrate. Anionic precursor stirring was switched on after five SILAR cycles.	4	3.05
No 2	Networked ZnO nanosheets on glass substrate coated with ZnO seeds. Anionic precursor stirring was switched on after five SILAR cycles.	6	3.05
No 3	ZnO nanorods on bare glass substrate. Anionic precursor stirring was switched on during all SILAR cycles.	8	3.13
No 4	Networked ZnO nanosheets on glass substrates coated with ZnO seeds. Anionic precursor stirring was switched on during all SILAR cycles.	16	3.16

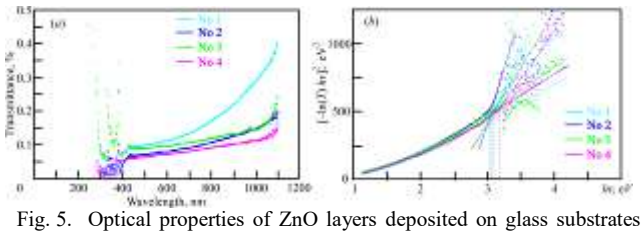

Fig. 5. Optical properties of ZnO layers deposited on glass substrates in different SILAR modes in samples No 1, No 2, No 3, and No 4: (a) – transmittance spectra T(λ); (b) – plots for estimating E_g

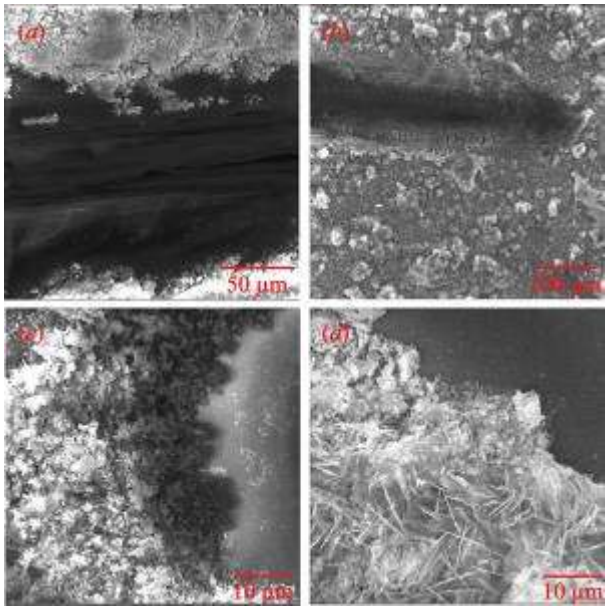

Fig. 6. SEM images after scratch testing performed using progressive loading for ZnO layers deposited by the SILAR method on bare glass substrates (sample No 3) (a,c) and on glass substrates coated with ZnO seed layers (sample No 4) (b,d) (both samples were made with continuous stirring of the anionic precursor during all SILAR cycles). Images in (a) and (b) represent scratch track at the middle stage of the testing. Images in (c) and (d) show the final stage of the scratch testing.

As seen in Fig. 6 (b), (c) and (d), cracks also appear ahead of the indenter. All these failures lead to through-thickness cracking at the front and sides of the indenter, which is conveniently called conformal cracking. Such film cracking under tensile stresses is characteristic of good adhesion of a brittle coating to a brittle substrate [16]. However, similar cracking was also observed in [17] for thin ZnO films grown by magnetron sputtering on a substrate of ductile superalloyed steel GH4169. In sample No 3 (Fig. 6 (a)), along with tensile cracking, Hertzian cracking is also observed. This confirms that the ZnO nanorods are more brittle than the networked ZnO nanosheets. SEM images in Fig. 6 (c) and (d) show chipping and loss of the ZnO layer at the final stage of testing at F_z above 10 N. According to [16], such delamination of the overlying brittle coating is a consequence of compressive stresses at very high loads in the case of good adhesion, when the coating bends into a scratch track and additional failure occurs within the brittle substrate. This once again confirms the good adhesion of both ZnO nanostructures deposited by the SILAR method on glass substrates.

Fig. 7 (a) shows the dependence of the indenter immersion depth Z during scratch testing carried out by applying a progressive load versus the time of indenter displacement for samples No 3 and No 4, as well as for an uncoated glass substrate. Fig. 7 (b) demonstrate corresponding dependences for normal force F_z on time of scratching. Fig. 8 shows graphs of normal force F_z, friction coefficient μ, and acoustic emission signal AE during these scratch testing. It is seen in Fig. 7 (a) a particularly sharp increase in the depth of the indenter immersion with time in the initial stage of the scratch testing for sample No 4 with networked ZnO nanosheets. The accelerated immersion of the intender into ZnO layers in Fig. 7 (a) corresponds to an abrupt decrease in the normal force F_z in its dependence on time in Fig. 7 (b). For the uncoated glass substrate, this effect was not observed; its dependences Z vs. time in Fig. 7 (a) and F_z vs. time in Fig. 7 (b) are directly proportional. Thus, fig. 7 indicates the destruction of both ZnO nanostructures in the first one and a half seconds of the scratch testing at a normal force of less than 3 N.

In Fig. 8 we can see a sharp increase in friction coefficients at the initial stage of scratch testing of both samples. For sample No 4, this is followed by a decrease in μ over about 1.5 seconds. Note that shortly after the start of scratch testing, the value of μ for sample No 3 in Fig. 8 (a) is two times lower than for sample No 4 in Fig. 8 (b). The explanation may be an abrasion and compaction of the nanostructured zinc oxide layers under the influence of compressive stresses at the beginning of the scratch testing, which, according to Figs. 7 and 8, was completed at F_z= 2.1 N in sample No 3 and at F_z= 2.6 N in sample No 4. According to the literature data [16-19], these values of normal forces correspond to larger critical loads L_c for networked ZnO nanosheets compared to the array of ZnO nanorods.

Moreover, at the initial stage the scratch testing of the ZnO layers the acoustic signal curves shown in Fig. 8 (a) and (b) are different. In Fig. 8 (a), the acoustic signals are more noticeable, since, according to [16], they correspond to both tensile and Hertzian cracks. In Fig. 8 (b) the acoustic signals are typical only for tensile cracks. Since, according to [16], all cracking events lead to some output of acoustic emission, it can be argued that in the first six seconds of testing, the array of ZnO nanorods was more prone to destruction than the networked ZnO nanosheets. As can be seen from Fig. 8, a sharp increase in the acoustic signal occurred for both samples No 3 and No 4 after 6 seconds of the scratch test, i.e. at F_z above 8 N. The generation of a large amount of acoustic emission in the scratch test is an indicator of interfacial failure by which the critical load for extensive coating detachment can be defined [16,17]. Thus, after 6 s of testing, at the stage of scratch testing at F_z above 8 N, the glass substrates were destroyed with simultaneous extensive delamination of ZnO.

The chipping and spallation events tested using the acoustic signal method were also observed by optical microscope and were shown in scratch micrographs in Fig. 8. At this stage of testing, a decrease in the friction coefficient of both samples was observed, but μ did not reach the value for an uncoated glass substrate, since the displacement of the intender required continuous destruction of the zinc oxide layer along the track.

ACKNOWLEDGMENTS

The authors are grateful to the Technical University of Liberec comprehensive assistance in carrying out the experiments.

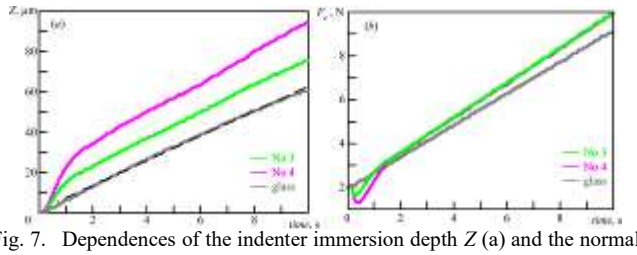

Fig. 7. Dependences of the indenter immersion depth Z (a) and the normal force F_z on time (b), obtained during scratching carried for samples No 3 and No 4, as well as for uncoated glass substrate.

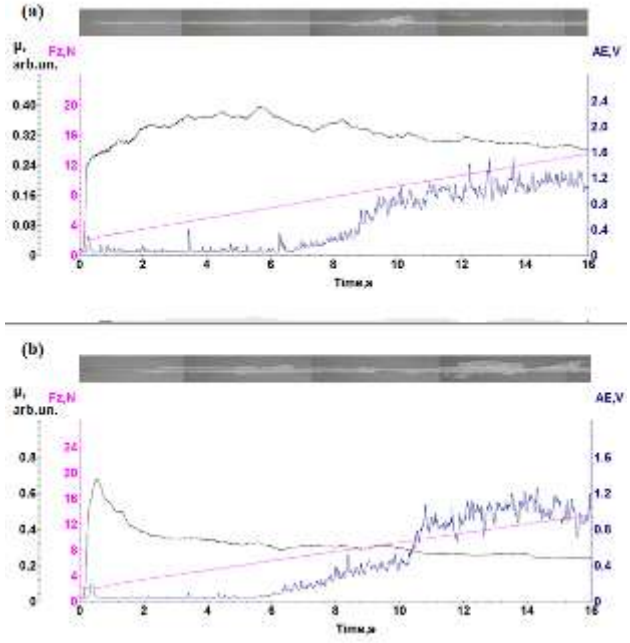

Fig. 8. Scratch micrographs and graphs of normal force F_z, friction coefficient μ, and acoustic emission signal AE versus the time of indenter displacement during the scratch testing performed by applying a linearly increasing load.. (a) –ZnO layer deposited by the SILAR method on bare glass substrate (sample No 3). (b) – ZnO layer deposited by the SILAR method on glass substrate coated with ZnIO seed layer (sample No 4)

IV. Conclusions

Herein, we demonstrated for the first time networked ZnO nanosheets fabricated by the automatic SILAR method using a ZnO seed layer at the initial stage of nucleation. It is shown that the automatic SILAR method developed here made it possible not only to obtain a promising 2D ZnO nanostructured material, but also offers the possibility of simple control of the geometric dimensions of ZnO nanosheets by changing the modes of solution stirring. The high adhesion of ZnO nanosheets to the glass substrate and their improved mechanical resistance were confirmed by scratch adhesion tests performed by applying a progressive load. It turned out that the normal force F_z = 2.6 N, corresponding to the critical load L_c, is greater for ZnO networked nanosheets than for ordinary ZnO nanorods, for which F_z = 2.1 N.

References

[1] S. Raha, M. Ahmaruzzaman, "ZnO nanostructured materials and their potential applications: progress, challenges and perspectives", Nanoscale Adv., 2022, vol. 4, pp. 1868–1925.

[2] A.A. Narasimulu, P. Zhao, N. Soin, K. Prashanthi, P. Ding, J. Chen, S. Dong, L. Chen, E. Zhou, C. D Montemagno, J. Luo, "Significant triboelectric enhancement using interfacial piezoelectric ZnO nanosheet layer", Nano Energy, 2017, vol. 40, pp. 471-480.

[3] K.-H. Kim, B. Kumar, K.Y. Lee, H.-K. Park, J.-H. Lee, H.H. Lee, H. Jun, D. Lee, S.-W. Kim, "Piezoelectric two-dimensional nanosheets/anionic layer heterojunction for efficient direct current power generation", Scientific Reports, 2013, vol. 3, pp. 2017-1–2017-6.

[4] H. Sun, M. Luo, W. Weng, K. Cheng, P. Du, G. Shen, G. Han, "Room-temperature preparation of ZnO nanosheets grown on Si substrates by a seed-layer assisted solution route", Nanotechnology, 2008, vol. 19, pp. 125603-1–125603-5.

[5] K. Sahu, S. Kuriakose, J. Singh, B. Satpati, S. Mohapatra, "Facile synthesis of ZnO nanoplates and nanoparticle aggregates for highly efficient photocatalytic degradation of organic dyes", Journal of Physics and Chemistry of Solids, 2018, vol. 121, pp. 186-195.

[6] F. Xu, Y. Lu, Y. Xie, and Y. Liu, "Controllable morphology evolution of electrodeposited ZnO nano/micro-scale structures in aqueous solution", Materials and Design, 2009, vol. 30, pp. 1704–1711.

[7] J. Demel, J. Pleštil, P. Bezdička, P. Janda, M. Klementová, K. Lang, ":Few-layer ZnO nanosheets: preparation, properties, and films with exposed {001} facets", The Journal of Physical Chemistry C, 2011, vol. 115, pp. 24702–24706.

[8] [8] S. Denchitcharoen, N. Siriphongsapak, P. Limsuwan, Growth of ZnO nanosheets by hydrothermal method on ZnO seed layer coated by spin-coating technique. Materials Today: Proceedings, 2017, vol. 4, pp. 6146–6152.

[9] O.F. Farhat, M.M. Halim, N.M. Ahmed, M.A. Qaeed, "ZnO nanofiber (NFs) growth from ZnO nanowires (NWs) by controlling growth temperature on flexible Teflon substrate by CBD technique for UV photodetector", Superlattices and Microstructures, 2016, vol. 100, pp. 1120-1127.

[10] S.P. Ratnayake, J. Ren, E. Colusso, M., Guglielmi, A. Martucci, E. Della Gaspera, "SILAR deposition of metal oxide nanostructured films", Small, 2021, vol. 17, pp. 2101666-1–2101666-32.

[11] N.P. Klochko, K.S. Klepikova, I.V. Khrypunova, V.R. Kopach, I.I. Tyukhov S.I. Petrushenko, S.V. Dukarov, V.M. Sukhov, M.V. Kirichenko, A.L. Khrypunova."Solution-processed flexible broadband ZnO photodetector modified by Ag nanoparticles", Solar Energy, 2022. vol. 232. pp. 1-11.

[12] N. Klochko, K. Klepikova, I. Khrypunova, V. Kopach, S. Petrushenko, D. Zhadan, S. Dukarov, V. Sukhov, M. Kirichenko, A. Khrypunova, "Flexible in-plane thermoelectric modules based on nanostructured layers ZnO and ZnO:In". Materials Today: Proceedings, 2022, vol. 62, pp .5729-5738.

[13] M.A. Gaikwad, M.P. Suryawanshi, P.S. Maldar, T.D. Dongale, A.V. Moholkar, "Nanostructured zinc oxide photoelectrodes by green routes M-SILAR and electrodeposition for dye sensitized solar cell", Optical Materials, 2018, vol. 78, pp. 325–334.

[14] M. Dehghanab, A. Behjat, "Deposition of zinc oxide as an electron transport layer in planar perovskite solar cells by spray and SILAR methods comparable with spin coating", RSC Adv., 2019, vol. 9, pp. 20917–20924.

[15] N.P. Klochko, K.S. Klepikova, S.I. Petrushenko, A.V. Nikitin, V.R. Kopach, I.V. Khrypunova, D.O. Zhadan, S.V. Dukarov, V.M. Lyubov, A.L. Khrypunova, "Effect of glow-discharge hydrogen plasma treatment on zinc oxide layers prepared through pulsed electrochemical deposition and via SILAR method", JNEP, 2019, vol. 11, pp. 05002-1–05002-7.

[16] S.J. Bull, "Failure modes in scratch adhesion testing", Surf. Coat. Technol., 1991, vol. 50, pp. 25–32

[17] G. Mo, Y. Cui, J. Yin, P. Gao, "Influence of ZnO film deposition parameters on piezoelectric properties and film-to-substrate adhesion on a GH4169 superalloy steel substrate", Micromachines, 2022, vol. 13, pp. 639-1-639-14.

[18] V.K. Belov, E.V. Gubarev, O.V. Krivko, A.V. Papshev, N.G. Gofman, E.G. Samorodova, "Determination of adhesive characteristics of coatings by application a modern scratch test. Part 1. Possibilities of application a modern scratch test to determine adhesion properties of coatings", Ferrous Metallurgy. Bulletin of Scientific, Technical and Economic Information, 2020. vol.76, pp. 143-152

[19] K. Moszak, A. Szczurek, B. Babiarczuk, B. Borak, J. Krzak, "ZnO sol-gel oxide coatings as materials for UV optical filters", Advanced Materials Letters, 2017, vol. 8, pp. 542–545.